IEEE Access
Multidisciplinary | Rapid Review | Open Access Journal

Received August 11, 2019, accepted September 18, 2019, date of publication September 23, 2019, date of current version October 15, 2019.

Digital Object Identifier 10.1109/ACCESS.2019.2943186

Unsupervised Segmentation of Choroidal Neovascularization for Optical Coherence Tomography Angiography by Grid Tissue-Like Membrane Systems

JIE XUE[1], SHUO YAN[1], YUAN WANG[1], TINGTING LIU[2], FENG QI[1], HONGYAN ZHANG[1], CHENGGONG QIU[1], JIANHUA QU[1], XIYU LIU[1], AND DENGWANG LI[3]

[1]Business School, Shandong Normal University, Jinan 250014, China
[2]Shandong Eye Hospital, Shandong Eye Institute, Shandong Academy of Medical Science, Jinan 250014, China
[3]Shandong Key Laboratory of Medical Physics and Image Processing, Shandong Provincial Engineering and Technical Center of Light Manipulation, School of Physics and Electronics, Shandong Normal University, Jinan 250014, China

Corresponding authors: Jianhua Qu (qjh@sdnu.edu.cn), Xiyu Liu (xyliu@sdnu.edu.cn), and Dengwang Li (lidengwang@sdnu.edu.cn)

This work was supported in part by the National Natural Science Foundation of China under Grant 61802234, Grant 61876101, and Grant 61971271, in part by the Natural Science Foundation of Shandong Province under Grant ZR2019QF007, in part by the China Postdoctoral Project under Grant 2017M612339, in part by the Natural Science Foundation for Distinguished Young Scholars of Shandong Province under Grant JQ201516, and in part by the Taishan Scholars Project of Shandong Province, Primary Research and Development Plan of Shandong Province, under Grant 2018GGX101018.

ABSTRACT Accurate segmentation of choroidal neovascularization (CNV) patterns is vital for precise lesion size quantification in age-related macular degeneration. In this paper, we develop a method for unsupervised and parallel segmentation of CNV in optical coherence tomography based on a grid tissue-like membrane (GTM) system. A GTM system incorporates a modified Clustering In QUEst (CLIQUE) algorithm into tissue-like membrane systems. Exploiting CLIQUE's aptitude for unsupervised clustering, GTM systems can detect CNV of different shapes, positions and density without the need of a training stage. The average dice ratio is 0.84±0.04, outperforms both baseline and the state-of-the-art methods. Besides, being a parallel computational paradigm, GTM systems can handle all scans under analysis simultaneously and therefore they are less time consuming, completing CNV detection on 48 scans in 0.56 seconds.

INDEX TERMS GTM systems, unsupervised segmentation, choroidal neovascularization, OCTA.

I. INTRODUCTION

Age-related macular degeneration (AMD) is the main cause of blindness for the elderly population in developed countries [1]. One of its manifestations is the neovascularization that breaks through the Bruch's membrane into the outer retina, a process known as choroidal neovascularization (CNV) [2]–[4]. In the past, fluorescein angiography (FA) or indocyanine green angiography (ICGA) have been used to detect CNV in the clinical practice. These techniques are invasive, involving intravenous dye injections [5], and cannot provide depth-resolved visualization of vasculature. Alternatively, optical coherence tomography (OCT) is a naturally three-dimensional imaging technique and the recent functional addition of OCT angiography (OCTA) can detect flow with high sensitivity at different retinal depths [6], [7], including flow in CNV [8], [9]. Although OCTA computes volumetric flow datasets, artifacts caused by projections cast by superficial flow onto deeper layers are observed in the outer retina, confounding interpretation of CNV. Therefore, automated discrimination of the pixels belonging to CNV vasculature from noise without manual intervention is a challenging task for the sake of accurate assessment of lesion size. Only few works [10], [11] focused on the automatic segmentation of CNV. Liu *et al.* [10] proposed a saliency-based algorithm to recognize CNV in OCTA outer retinal *en face* angiograms. This method could detect the CNV area with an accuracy of 83% on 7 subjects. We have previously proposed density cell-like P systems with active membranes to improve the accuracy of recognition of CNV area to 87%

The associate editor coordinating the review of this manuscript and approving it for publication was Eduardo Rosa-Molinar.

on 22 subjects [11]. However, both of the above two methods could not distinguish between distinct vessels forming the CNV vascular pattern or detect the CNV boundaries with precision. Moreover, they must employ methods in [12] to remove artifacts, which increased the computational complexity of the algorithms.

In order to design an algorithm with the ability to find arbitrary groups and discriminate noise pixels with high flow signal from the pixels in the CNV vascular pattern, clustering method can be used. Clustering is an unsupervised machine learning paradigm designed for classification of pixels with similar characteristics without any prior knowledge of the dataset nor need for a training stage [13]. Clustering algorithms can be based on the connectivity of points (hierarchical clustering), the distance from cluster centroids (e.g. k-means or fuzzy c-means), distribution models or density of points (e.g. DBSCAN). Clustering In QUEst (CLIQUE) is an example of a grid-density based clustering algorithm, which has both the advantages of grid and density clustering [14]. CLIQUE reduces the time consumption in density clustering by searching data based on grids [15]. Unlike partitioned clustering algorithms and hierarchical algorithms, which need to either input the number of clusters before computing or select the expected shapes of groups, CLIQUE has the ability to discover groups with arbitrary shapes and, therefore, it is suitable for detecting individual CNV vessels in OCTA. However, clustering algorithms such as CLIQUE are time consuming. They need to read the dataset in each dimension, do self-joining of every unit, and require trial and error to determine the appropriate length and sensitivity of units.

To alleviate these problems and improve the effectiveness of CLIQUE, it can be implemented in a parallel computation scheme that can scan all dimensions in different membranes simultaneously. Membrane computing, initiated by Păun [16], is a computational model that encapsulates the data in arrangements of ''membranes'' that communicate under certain rules with a given computational purpose. Membrane computing has been applied on the segmentation of digital images [17]–[19] as well as in various fields such as language generation, electricity fault diagnosis, and combination optimization [1], [20]–[24]. Clustering based on membrane systems has shown good convergence, robustness, and parallelism [25]–[29]. In image processing applications, membranes can operate in parallel in different local areas independently of the image size [30]. In particular, the tissue-like membrane system (TMS) is a particularly flexible network membrane structure that is adaptable to various network topologies [31], [32]. TMSs have a network membrane structure consisting of several one-membrane cells in a common environment and a certain number of channels connecting the cells. These features become very useful in organizing the CLIQUE algorithm for detection of CNV architectures with different characteristics of vascular pixel distribution.

Based on the above considerations, we formulate here a grid tissue-like membrane (GTM) system, which consists of a modified CLIQUE clustering algorithm implemented in a tissue-like membrane system, and apply it to the detection of CNV vascular patterns in OCTA images. Specifically, we use the GTM system to find a cluster of pixels contained in the largest number of grid units, representing the location of CNV vasculature. The proposed method can distinguish CNV vasculature from surrounding noise better than previous methods, has the ability to discover clusters with arbitrary shapes. The average dice ratio of our method for CNV is 0.84, which is the best result to date.

The contributions of our work can be summarized as follows:

(1) GTM systems integrate clustering algorithm into tissue-like membrane systems, with the goal of making full use of the excellent convergence, robustness and parallelism of membrane systems as well as the good performance of clustering algorithm for CNV segmentation. New types of rules are also designed to solve complex real applications.

(2) A modified CLIQUE algorithm is proposed to be implemented in GTM system for more accurate clustering. In particular, effective data points and new search path are defined in the identification and grouping of dense units to deal with the abundant noise around CNV vascular pattern.

(3) Compared to detection of CNV area based on removing artifacts by other methods, our approach yields CNV vascular pattern segmentation directly. Detailed lesion identification may significantly help doctors achieve early and accurate diagnosis.

II. PROBLEM STATEMENT

Clustering is to divide a set of objects, where objects in the same group are more similar to each other than them to objects in different groups. The segmentation of CNV vascular pattern in OCTA can be viewed as a clustering problem, where one cluster is the target lesion and the others are backgrounds. The combination of clustering and membrane systems showed good performance [25]–[29]. TMS [31], [32] is a classic type of membrane system, which associates a graph structure consisting of nodes corresponding to cells and the environment and edges that represent channels linking various components.

A TMS (Fig. 1) with symport/antiport rules is formally defined as a tuple:

$$\prod = \left(O, w_1, \ldots, w_q, R_1, \ldots, R_q, i_0\right), \tag{1}$$

where O is a finite set of objects; $w_1, \ldots, w_q$ are initial multisets of objects; $i_0 \in \{0, 1, \ldots, q\}$ indicates the output cells of the system. R_i are finite sets of symport/antiport rules in cell i; and $1 \leq i \leq q$. A symport rule has the form $(i, u/\lambda, j)$, which means that the multiset of objects u goes from cell i to cell j. An antiport rule has the form $(i, u/v, j)$, indicating that the multiset of objects u in cell i and the multiset of objects v in cell j are interchanged.

The tissue-like P system starts with the initial multisets $w_1, \ldots, w_q$. Then, in each step, the symport and antiport rules are applied in the maximally parallel manner (a maximal multiset of applicable rules is non-deterministically chosen

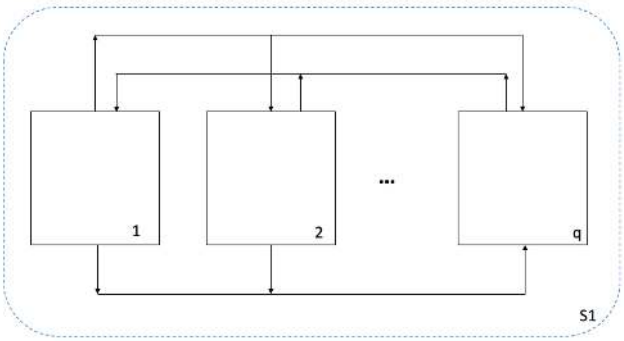

FIGURE 1. Membrane structure of tissue-like membrane system. S1 is the environment, which has no membranes outside. 1...q are q numbers of computing membranes.

and applied). This process is repeated until a termination condition is satisfied. When it terminates, final result is embodied by the output cells.

III. CNV VASCULAR PATTERN RECOGNITION BY GTM SYSTEMS

Inspired by CLIQUE algorithm and TMS, we propose GTM systems to detect CNV vessels. The flowchart of the proposed method is shown in Fig. 2. The purpose of GTM systems is to find the set with the maximum number of adjacent dense units (defined below), which represents a cluster of CNV pixels.

Since OCTA are 2-dimensional images, we implemented the modified CLIQUE algorithm in a space of 2-dimensional points. The input consists of a set of 2-dimensional set of non-zero pixels $V = \{v_1, v_2, \ldots, v_n\}$, where $v_i = \{v_{i1}, v_{i2}\}$, $1 \leq i < n$ and v_{i1}, v_{i2} are coordinates of point v_i. Because noise is abundant and CNV pixels are closer to each other than noise pixels, we applied an additional filtering step based on the Euclidean distance information between pixels to reduce the number of noise pixels in the computation of GTM.

The Euclidean distance between two pixels v_α and v_β, $\alpha, \beta \in \{1, 2, \ldots, n\}, i \neq j$ is computed by Eq.(2) and the set $S = \{dis(v_\alpha, v_\beta)\}$ corresponding to the set of distances between any two pixels is saved.

$$dis(v_\alpha, v_\beta) = \sqrt{(v_{i1\alpha} - v_{i2\alpha})^2 + (v_{i1\beta} - v_{i2\beta})^2} \qquad (2)$$

Rather than using all non-zero pixels in the identification of dense units, we define effective data points, which are all pixels v_α whose Euclidean distance to the closest non-zero pixel v_β is less than an input parameter τ.

Then, each dimension of OCTA is partitioned into ζ intervals of equal length, forming non-overlapping units. A 2-dimensional unit σ has the form $\{\sigma_1, \sigma_2\}$, where $\sigma_j = [l_j, h_j)$, $1 \leq j \leq 2$ is a right-open interval in the partition. A pixel v_i is contained in a unit σ if its location in both j dimensions is within the interval $l_j \leq v_{ij} < h_j$. A unit σ is considered to be dense if it contains a number Q of effective points with $Q > \theta$, where θ is defined before computation according to the distribution of CNV pixels. After all dense units have been recognized, the unit σ_F with the maximal number of adjacent dense units is selected.

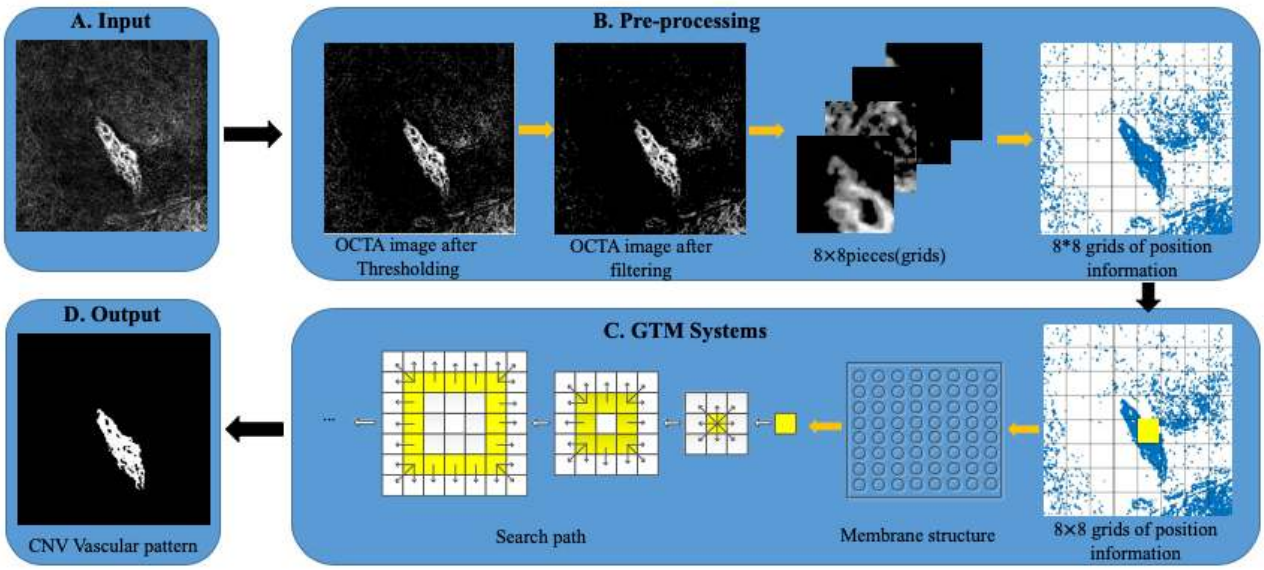

FIGURE 2. Description of the proposed method. In block (A), the OCTA image is acquired. In Block (B), a threshold is set first to remove low flow signal pixels and a median filtering is used to smooth the OCTA image. 8×8 units are used to partition the filtered angiogram. The rightmost image in block (B) represents the positions of all non-zero pixels and the grid units where they are located. In Block (C), a GTM-systems-based algorithm is used to segment CNV vascular patterns. The densest unit is first detected (highlighted in yellow) and assigned to a membrane in a membrane structure formed by a skin membrane containing as many inner membranes as units in the grid. Adjacent membranes within the structure can communicate with each other. The last figure of Block (C) depicts the search path method. Each unit is considered to be dense if the amount of effective data points in it is larger than a certain threshold. After all dense units have been recognized, the unit with the maximal number of adjacent dense units is selected, which is highlighted in yellow. This unit and its adjacent dense units are chosen as the first members of cluster *C*. Then, each unit in *C* is set as a start unit to search whether its outer neighbors are also dense, in order to be added to *C*. When the search ends, the clusters are extracted and the vascular pattern is found in the cluster with the largest number of units.

Two 2-dimensional dense units are adjacent if they have a common face or if there exists another 2-dimensional dense unit adjacent to both. Then, σ_F and its adjacent dense units are chosen as the first members of cluster C. Then, each unit in C is set as a start unit to search whether its outer neighbors are dense. If they are dense, they will be added to C (Fig. 2, search path). The algorithm terminates when no more units are searched and the cluster with the maximal set of adjacent dense units is output as the collection of units containing the CNV pixels.

Next, we propose a GTM system as a parallel implementation of CLIQUE for the detection of the CNV pixels. A GTM system is a kind of tissue-like P system (TMS) [23]. TMS has graph based membrane structures, which is a flexible network topology with several one-membrane cells in a common environment and a certain number of channels connecting the cells. Each cell contains multisets of objects and communicates with each other through the communication rules in parallel.

The structures and ways of communication of TMS is suitable for finding adjacent dense units and implementing the search path in the detection of CNV architectures.

A GTM system for the detection of the CNV pixels is a construct of the form:

$$\prod = \{O, \lambda, q, \sigma, \sigma_0, \omega, R_i\} \tag{3}$$

The finite non-empty alphabet is $O = \{V, S, \zeta, \tau, \theta\}$; λ denotes an empty object; q is the initial number of cells, $\sigma = \{\sigma_1, \sigma_2, \ldots, \sigma_q\}$ is the set of cells, excluding σ_0, which is the environment. The membrane structure is shown in Block (C) of Fig. 2. $\omega = \{i, V_i, S_i, \tau, \theta\}$ are initial multisets of objects in every cell σ_i ; Any two cells σ_i and σ_j representing units σ_i and σ_j contain objects, can communicate with each other and are subjected to rules R_i defined below:

$$(\sigma_i, \{i, V_i, S_i, \tau, \theta\}/\sigma_i, \lambda), S_i > \tau \tag{4}$$

$$(\sigma_i, \{i, V_i, S_i, \tau, \theta\}/\sigma_j, \{i, V_i, S_i, \tau, \theta\}) \tag{5}$$

$$(\sigma_F, \{g^{\max}, F, V_F, S_F, \tau, \theta\})/\sigma_F, C) \tag{6}$$

$$(\sigma_i, \{i, V_i, S_i, \tau, \theta, C\} \rightarrow \sigma_0, \{i, V_i, S_i, \tau, \theta, C\}) \tag{7}$$

$$(\sigma_i, \{i, V_i, S_i, \tau, \theta, C\} \rightarrow \sigma_0, \{i, V_i, S_i, \tau, \theta, C\}) \tag{8}$$

Rule Eq. (4) removes objects from cell σ_i if they are non-effective data points in unit μ_i considering the distance threshold τ. Eq. (5) communicates dense units with their adjacent dense units. Eq. (5) sends $\{i, V_i, S_i, \tau, \theta\}$ to another cell σ_j connected with σ_i within σ_0. Eq. (6) obtains cell σ_F .Variable $g^{\max}$ counts the number of units adjacent to σ_F . Eq. (6) also produces a new object C, which means unit σ_F belongs to cluster C. If units outside C are dense and adjacent to dense units within C, they are incorporated to C by Eq. (7). 'out' means multiset $\{i, V_i, S_i, \tau, \theta, C\}$ will be sent to σ_0 from cell σ_i . Eq. (8) outputs all cells that have object C.

The process halts when there are no rules being activated. When the system halts, all the objects in the output cell σ_0 are regarded as the final solution of the GTM system.

IV. EXPERIMENTAL RESULTS AND DISCUSSION

A. DATA ACQUISITION

OCTA data was acquired from 48 patients with neovascular AMD recruited at the Shandong Eye Hospital, Shandong Eye Institute. The image size is 465×465, acquired on SPECTRALIS HRA+OCT Multicolor with OCT2 Module (Heidelberg Engineering GmbH, Germany). Manual segmentation of CNV vascular pattern by two experienced graders are deemed as ground-truth.

B. PRE-PROCESSING

First, a threshold at 0.3 is imposed to reduce noise while preserving the CNV structure and a median filter with 3×3-pixel kernel is applied in order to smooth images. Then, we extract the position of all remaining non-zero pixels $v_i = (v_{i1}, v_{i2})$, $1 \leq i \leq 465$.

C. PARAMETERS SETTING

There are three initialization parameters: $\zeta = 58$ is the interval size of units, $\tau = 5$ is the maximum distance between effective points and $\theta = 25$ is the minimum number of effective data points necessary to consider σ dense. 48 scans from subjects with neovascular AMD were processed in MATLAB 2017a (MathWorks, Natick, MA) on an Intel Xeon(R) CPU (3.30GHz×4) simultaneously due to the parallelism of GTM systems. The time invested to process all subjects was only 0.56 s.

D. EVALUATION METRICS

Results obtained from GTM systems were compared with manual results by computing the dice ratio, accuracy, false negative rate (FNR) and false positive rate (FPR). Dice ratio is defined between GTM (G) and manual (M) images as:

$$dice = \frac{2\times \parallel G \cap M \parallel}{\parallel G \cap M \parallel} \tag{9}$$

Accuracy was calculated by Eq. (10) from the number of true positive (TP), true negative (TN), false positive (FP) and false negative (FN) pixels.

$$Accuracy = \frac{TP + TN}{TP + FP + TN + FN} \tag{10}$$

FNR and FPR measure the fractions of relevant segmented pixels. The definitions of these metrics are given below:

$$False\ negative\ rate = \frac{FN}{TP + FN} \tag{11}$$

$$False\ positive\ rate = \frac{FP}{FP + TN} \tag{12}$$

The true positive (TP) score reflects the number of vascular pixels correctly identified as vascular pixels. The false positive (FP) score reflects the number of non-vascular pixels incorrectly identified as vascular pixels. The true negative (TN) score reflects the number of background pixels correctly identified as background pixels. Finally, the false negative (FN) score reflects the number of non-background pixels incorrectly identified as background pixels.

E. COMPARISON WITH THE STATE-OF-THE-ART METHODS

In this subsection, we compare the performance of our proposed method for the segmentation of CNV vascular pattern with the two state-of-the-art methods briefly introduced below.

Liu *et al.* [10] proposed a saliency-based algorithm to recognize CNV area in OCTA outer retinal *en face* angiograms.

Xue *et al.* [11] employed DBScan algorithm in cell-like P system with active membranes to improve the accuracy of recognition of CNV area.

Table 1 compares the segmentation performance of our proposed method with two state-of-the-art methods, using mean dice ratio, accuracy, FNR and FPR (with standard deviation).

Dice ratio and accuracy over 48 samples increase from 0.65 to 0.84 and 0.91 to 0.96. FNR and FPR decrease from 0.25 to 0.23, and 0.14 to 0.03, compared to the state-of-the-art methods. Four examples of the ground-truth and our segmentations are shown in Fig. 3. As can be observed from Fig. 3, the similarity with manual

TABLE 1. Quantitative comparisons of Dice, Accuracy, FNR, and FPR for CNV vascular pattern segmentation on the OCTA images of 48 subjects. (The best results are indicated in bold, mean ± std).

Method	No.	Dice	Accuracy	FNR	FPR
Liu et al.[10]	48	0.26±0.21	0.86±0.06	0.69±0.04	0.09±0.02
Xue.et al.[11]	48	0.65±0.04	0.91±0.06	0.25±0.06	0.14±0.03
Our proposed method	48	**0.84±0.04**	**0.96±0.02**	**0.23±0.08**	**0.03±0.02**

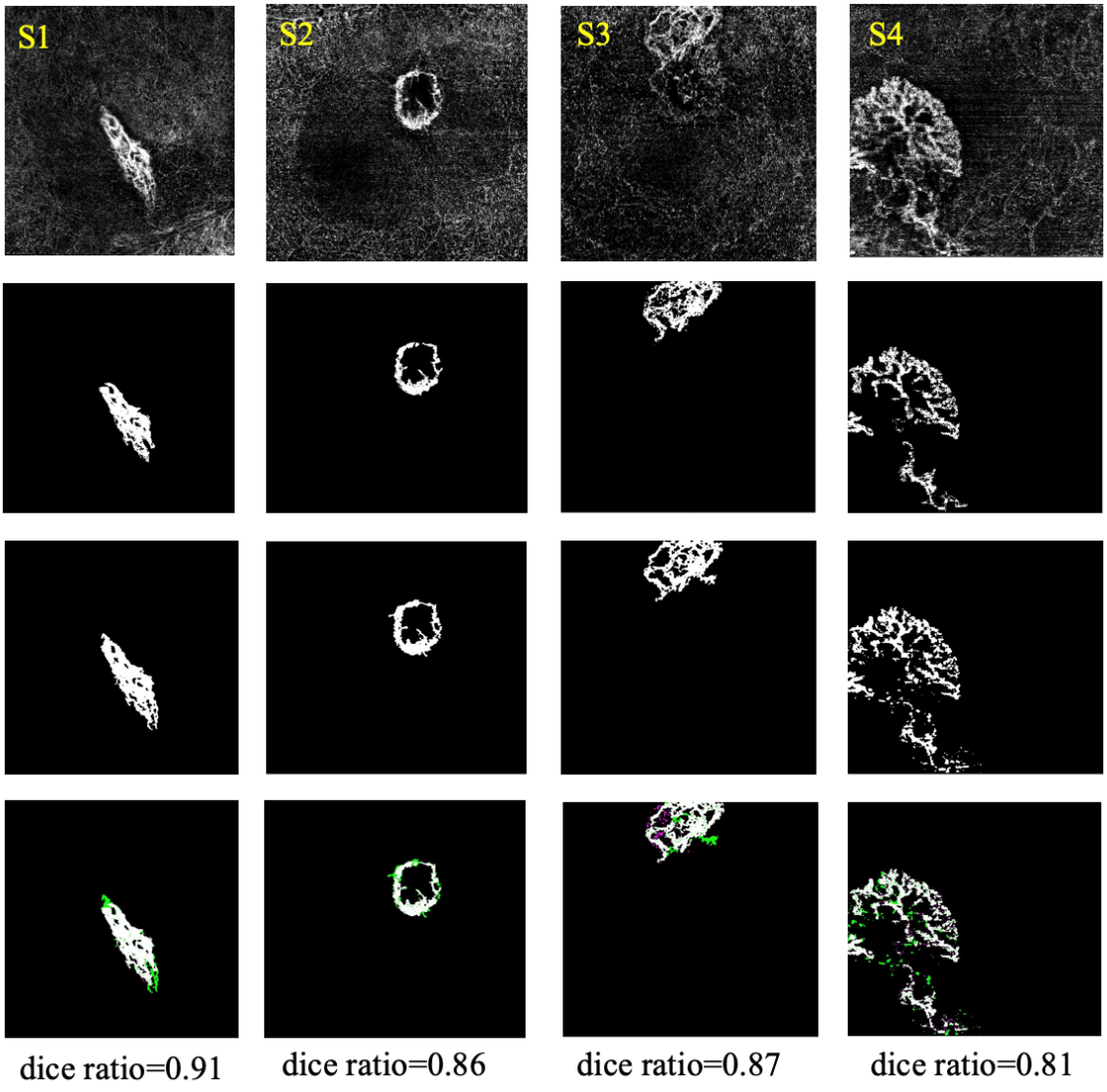

FIGURE 3. CNV vascular pattern segmentation results for four examples (S1, S2, S3 and S4). The first row shows the OCTA, and the second row shows the final segmentation results, the third row shows the ground-truth segmentations and the last row shows the compared results between our segmentation results and the ground-truth segmentations. Pink results show the under-segmentation of GTM system compared with the ground-truth Segmentations. And Green results show the over-segmentation of GTM system compared with the ground-truth segmentations.

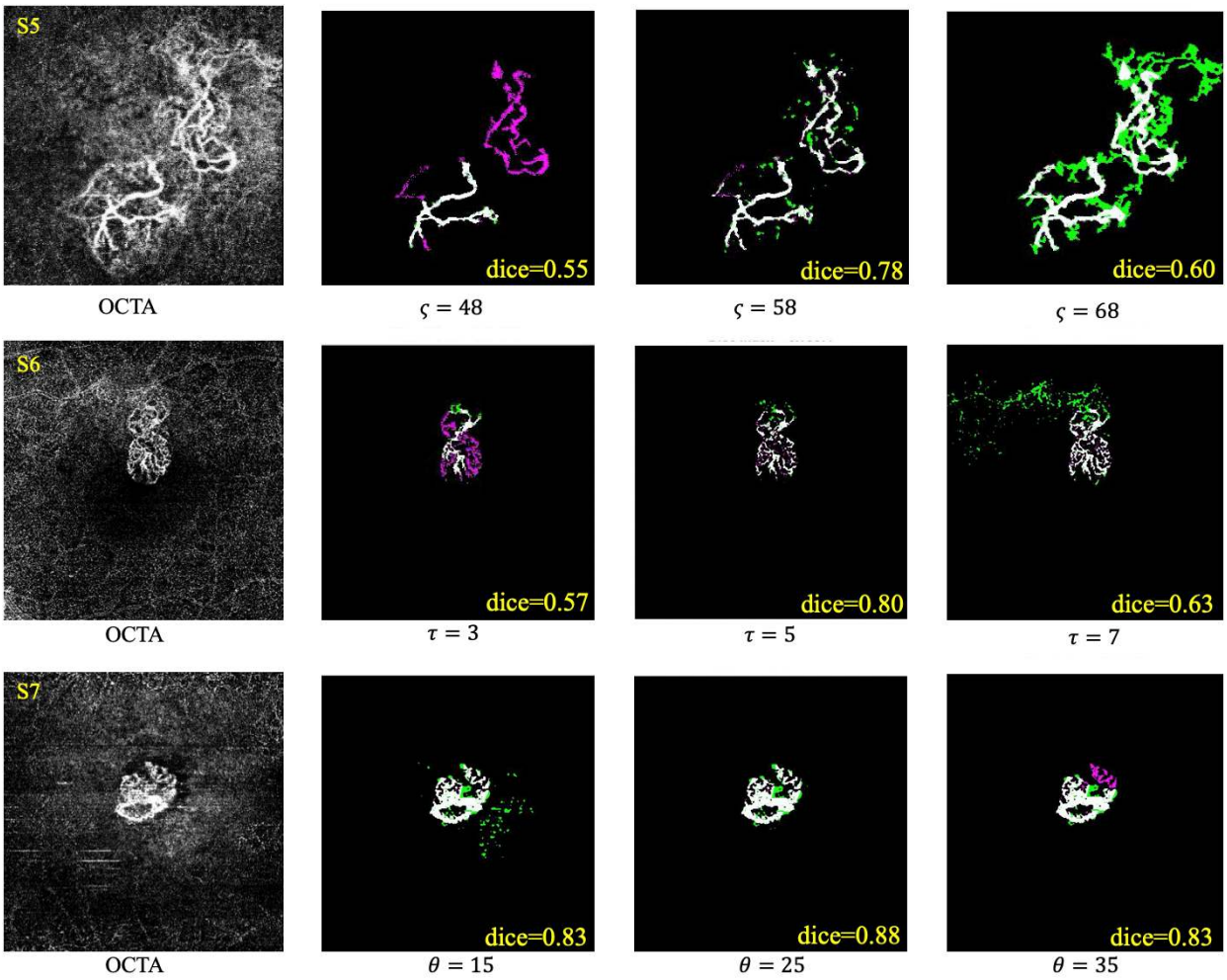

FIGURE 4. Qualitative comparison of the results of GTM system with different parameters to manual grading on three cases (S5, S6, S7). Pink results show the under-segmentation of GTM system compared with the manual grading. And Green results show the over-segmentation of GTM system compared with the manual grading.

grading is higher by our proposed method, in spite of diverse shapes and locations of CNV vessels in OCTA images.

Moreover, although manual grading was used as reference for performance evaluation, the grader cannot remove noise contained within the CNV membrane area. Since the GTM system removes noise pixels by elimination of non-effective points from membranes and hence, never promoting them to a cluster C, manual grading and GTM system would differ at these points. For this reason, the false negative rate was significantly higher than the false positive rate, indicating that there is a limitation in the accuracy of manual grading for performance assessment.

To further evaluate the contribution of the modified CLIQUE algorithm in GTM system, we also compared it with the unmodified version. The four indices over 48 samples are 0.77 ± 0.06, 0.93 ± 0.06, 0.23 ± 0.08, 0.20 ± 0.05. Therefore, our proposed method with the modified CLIQUE algorithm improves the segmentation accuracy significantly.

F. EVALUATION ON THE IMPACT OF THE INTERVAL SIZE OF UNITS

Since different interval sizes of the units (i.e. the initial number of membranes) change the effective points in each unit which contributes to different cluster accuracies, we conduct experiments using three different interval sizes of the units, i.e., 48, 58 and 68. As shown in Fig. 4 (S5) and Fig. 5, our method obtains the best results with $\zeta = 58$. Due to the small interval size, the effective points decrease in each unit, the performance is with high under-segmentation. On the contrary, large interval size causes redundant noises in each unit, leading to over-segmentation.

G. EVALUATION ON THE IMPACT OF THE MAXIMUM DISTANCE BETWEEN EFFECTIVE POINTS

To find a maximum distance that ensures the number of effective points in their units and minimum the number of noises, we set the maximum distance as 3, 5, 7 for testing.

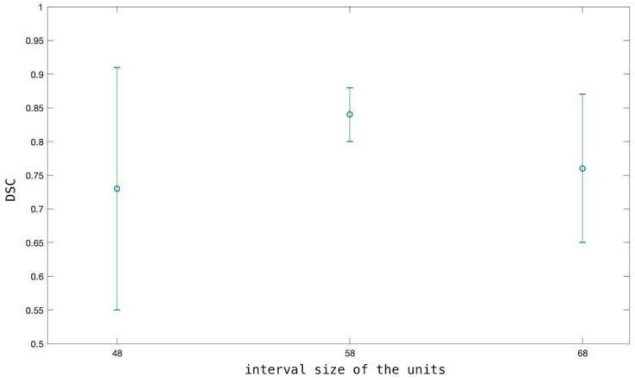

FIGURE 5. Changes of values of dice ratio with respect to three different interval sizes. The first bar, second bar and last bar correspond to the sizes of 48, 58 and 68, respectively.

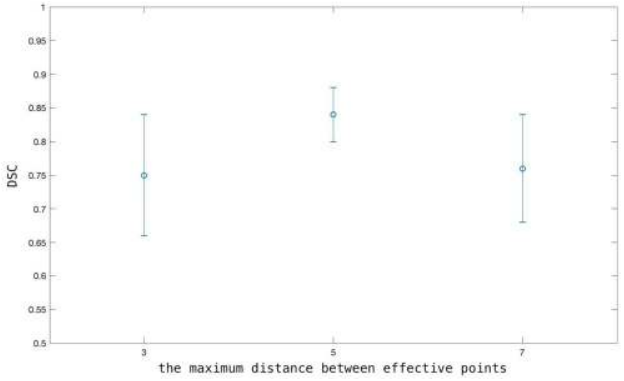

FIGURE 6. Changes of values of dice ratio with respect to three different maximum distance. The first bar, second bar and last bar correspond to the distances of 3, 5 and 7, respectively.

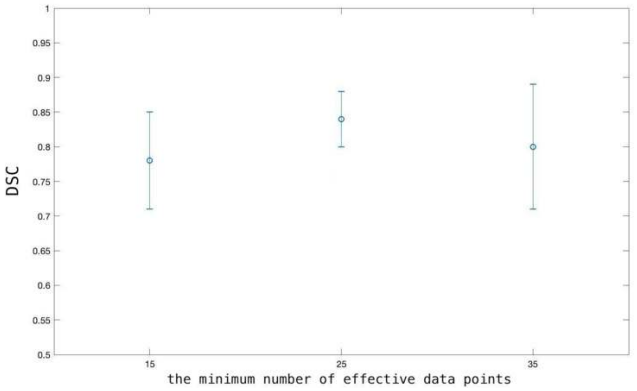

FIGURE 7. Changes of values of dice ratio with respect to three different minimum number of effective data points. The first bar, second bar and last bar correspond to the number of 15, 25 and 35, respectively.

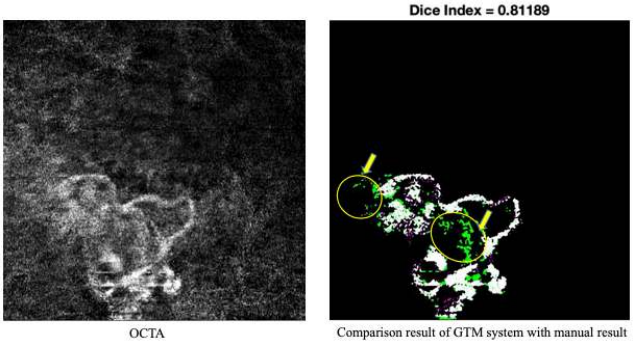

FIGURE 8. Performance of the GTM systems compared to manual delineation in the scan that noise pixels are bright and found within the vicinity of vessels. Yellow arrows direct to noise pixels in yellow circles.

Small distance increases the workload and costs more time. The performance results are given in Fig. 4 (S6) and Fig. 6. The maximum distance of 5 obviously perform better than the others. Therefore, we select $\tau = 5$ for experiments.

H. EVALUATION ON THE IMPACT OF THE MINIMUM NUMBER OF EFFECTIVE DATA

We also compared the proposed method on three different minimum number of effective data points, i.e., 15, 25, 35. Similar to maximum distance, the minimum number of effective data points also contribute to the selection of dense units. As can be seen in Fig. 4 (S7) and Fig. 7, $\theta = 25$ are the best choices for the detection of CNV vessels for all the 48 cases.

I. EVALUATION ON IMAGES WITH LOW QUALITY

Sine the proposed method does not need to employ additional methods, like [12] to remove artifacts, which decreased the computational complexity of the algorithms. To further verify the effectiveness of the proposed method on images with low quality, we also conduct our experiments on OCTA images with noise pixels that are bright and found within the vicinity of vessels. As can be seen in Fig. 8, the proposed method can also segment CNV vessels accurately. But noise pixels as high as pixels in CNV and located in the same grid cannot be removed. After confirmed by clinicians, the segmentation is significant in helping them diagnose and treat patients with CNV.

TABLE 2. The p-values of our method compared to the other methods for the results in Table 1.

Method	p_{Dice}	$p_{Accuracy}$	p_{FNR}	p_{FPR}
Liu et al.[10]	$1.8*10^{-30}$	$2.2*10^{-17}$	$1.2*10^{-57}$	$2.3*10^{-25}$
Xue.et al.[11]	$1.7*10^{-19}$	$1.8*10^{-10}$	0.08	$1.5*10^{-38}$

J. STATISTICAL SIGNIFICANCE TEST

We compared our results with those of previous methods using t-tests. The p-values for the dice ratio, accuracy, FNR, FPR of CNV were all <0.001 (Table 2) compared with methods [10]. The p-values for dice ratio, accuracy, FPR (Table 2) are also p<0.001 compared with methods [11]. Therefore, our proposed method leads to highly significant improvements (p<0.001) in the ability to correctly detect CNV vessels compared with the methods in [10], [11].

TABLE 3. Running time of our method compared to other methods.

Method	No.	Time
Liu et al.[10]	48	1117.2 s
Xue.et al.[11]	48	82.3 s
CLIQUE algorithm without membrane systems	48	429.9 s
Our proposed method	48	**0.56 s**

K. RUNNING TIME OF GTM SYSTEMS

Table 3 provides the running time of GTM systems, method in [10], method in [11] and CLIQUE algorithm without membrane systems, which shows that GTM systems can improve the efficiency of CNV vessels segmentation.

V. CONCLUSION

We have reported an automatic detection algorithm for CNV in AMD. We treat the vessel segmentation problem as a clustering problem and implement a modified CLIQUE clustering into a tissue-like membrane computing model, which we call a GTM system, to identify vascular patterns. Compared with the CLIQUE clustering algorithm, the GTM system handles all cases synchronously and guarantees convergence. Unconcerned about the size of dataset, the GTM system can be performed in parallel in different local areas, which reduces time consumption and improves efficiency. The GTM model can complete the segmentation task in a population of 48 subjects in less than a second. Good accuracy and similarity to the results from human grading were obtained. The algorithm was characterized by high computational speed, guaranteed convergence and high detection accuracy, which indicates the effectiveness of proper hybridization of a tissue membrane system with conventional methods. It also suggests a promising way toward the improvement and biological realization of several machine learning methods by using membrane systems. Our future work will focus on the applications of this hybrid approach to more problems.

REFERENCES

[1] H. Peng, J. Wang, J. Ming, P. Shi, M. J. Pérez-Jiménez, W. Yu, and C. Tao, "Fault diagnosis of power systems using intuitionistic fuzzy spiking neural P systems," *IEEE Trans. Smart Grid*, vol. 9, no. 5, pp. 4777–4784, Sep. 2018.

[2] R. D. Jager, W. F. Mieler, and J. M. Miller, "Age-related macular degeneration," *New England J. Med.*, vol. 358, no. 24, pp. 2606–2617, 2008.

[3] Min Zhao, I. Mantel, E. Gelize, X. Li, X. Xie, A. Arboleda, M. Seminel, R. Levy-Boukris, M. Dernigoghossian, A. Prunotto, C. Andrieu-Soler, C. Rivolta, J. Canonica, M.-C. Naud, S. Lechner, N. Farman, I. Bravo-Osuna, R. Herrero-Vanrell, F. Jaisser, and F. Behar-Cohen, "Mineralocorticoid receptor antagonism limits experimental choroidal neovascularization and structural changes associated with neovascular age-related macular degeneration," *Nature Commun.*, vol. 10, p. 369, Jan. 2019.

[4] A. Barros, J. Chibante-Pedro, and L. Duarte, "Choroidal neovascularization after blunt ocular trauma: OCT Angiography better than fluorescein angiography for diagnosis and treatment follow-up," *Vis. Pan-Amer., Pan-Amer. J. Ophthalmol.*, vol. 17, no. 1, pp. 31–35, 2018.

[5] Y. Jia, S. T. Bailey, D. J. Wilson, O. Tan, M. L. Klein, C. J. Flaxel, B. Potsaid, J. J. Liu, C. D. Lu, M. F. Kraus, J. G. Fujimoto, and D. Huang, "Quantitative optical coherence tomography angiography of choroidal neovascularization in age-related macular degeneration," *Ophthalmology*, vol. 121, no. 7, pp. 1435–1444, Jul. 2014.

[6] Y. Jia, O. Tan, J. Tokayer, B. Potsaid, Y. Wang, J. J. Liu, M. F. Kraus, H. Subhash, J. G. Fujimoto, J. Hornegger, and D. Huang, "Split-spectrum amplitude-decorrelation angiography with optical coherence tomography," *Opt. Express*, vol. 20, no. 4, pp. 4710–4725, 2012.

[7] Q. Zhang, C.-L. Chen, Z. Chu, F. Zheng, A. Miller, L. Roisman, J. R. de Oliveira Dias, Z. Yehoshua, K. B. Schaal, W. Feuer, G. Gregori, S. Kubach, L. An, P. F. Stetson, M. K. Durbin, P. J. Rosenfeld, and R. K. Wang, "Automated quantitation of choroidal neovascularization: A comparison study between spectral-domain and swept-source OCT angiograms," *Investigative Ophthalmol. Vis. Sci.*, vol. 58, no. 3, pp. 1506–1513, 2017.

[8] R. F. Spaide, "Optical coherence tomography angiography signs of vascular abnormalization with antiangiogenic therapy for choroidal neovascularization," *Amer. J. Ophthalmol.*, vol. 160, no. 1, pp. 6–16, Jul. 2015.

[9] L. Kuehlewein and S. R. S. Sarraf, "OCT angiography and sequential quantitative analysis of type 2 neovascularization after ranibizumab therapy," *Eye*, vol. 29, no. 7, pp. 932–935, 2015.

[10] L. Liu, S. S. Gao, S. T. Bailey, D. Huang, D. Li, and Y. Jia, "Automated choroidal neovascularization detection algorithm for optical coherence tomography angiography," *Biomed. Opt. Express*, vol. 6, no. 9, pp. 3564–3576, 2015.

[11] J. Xue, A. Camino, S. T. Bailey, X. Liu, D. Li, and Y. Jia, "Automatic quantification of choroidal neovascularization lesion area on OCT angiography based on density cell-like P systems with active membranes," *Biomed. Opt. Express*, vol. 9, no. 7, pp. 3208–3219, 2018.

[12] M. F. Kraus, B. Potsaid, M. A. Mayer, R. Bock, B. Baumann, J. J. Liu, J. Hornegger, and J. G. Fujimoto, "Motion correction in optical coherence tomography volumes on a per A-scan basis using orthogonal scan patterns," *Biomed. Opt. Express*, vol. 3, no. 6, pp. 1182–1199, 2012.

[13] A. K. Jain, M. N. Murty, and P. J. Flynn, "Data clustering: A review," *ACM Comput. Surv.*, vol. 31, no. 3, pp. 264–323, 1999.

[14] R. Agrawal, J. Gehrke, D. Gunopulos, and P. Raghavan, "Automatic subspace clustering of high dimensional data for data mining applications," in *Proc. ACM SIGMOD Int. Conf. Manage. Data*, Jun. 1998, pp. 94–105.

[15] H. Zhang and X. Liu, "A CLIQUE algorithm using DNA computing techniques based on closed-circle DNA sequences," *Biosystems*, vol. 105, no. 1, pp. 73–82, 2011.

[16] G. Paŭn, "Computing with membranes," *J. Comput. Syst. Sci.*, vol. 61, no. 1, pp. 108–143, Aug. 2000.

[17] D. Díaz-Pernil, M. A. Gutiérrez-Naranjo, and H. Peng, "Membrane computing and image processing: A short survey," *J. Membrane Comput.*, vol. 1, no. 1, pp. 58–73, Mar. 2019.

[18] J. Xue, S. Yan, J. Qu, F. Qi, C. Qiu, H. Zhang, M. Chen, T. Liu, D. Li, and X. Liu, "Deep membrane systems for multitask segmentation in diabetic retinopathy," *Knowl.-Based Syst.*, vol. 183, Nov. 2019, Art. no. 104887. doi: 10.1016/j.knosys.2019.104887.

[19] H. A. Christinal, D. Díaz-Pernil, and P. R. Jurado, "Segmentation in 2D and 3D image using tissue-like P system," in *Proc. Iberoamerican Congr. Pattern Recognit.*, 2009, pp. 169–176.

[20] M. Campos, R. Capilla, F. Naya, R. Futami, T. Coque, A. Moya, V. Fernandez-Lanza, R. Cantón, J. M. Sempere, C. Llorens, and F. Baquero, "Simulating multilevel dynamics of antimicrobial resistance in a membrane computing model," *Ecol. Evol. Sci.*, vol. 10, no. 1, 2019, Art. no. e02460. doi: 10.1128/mBio.02460-18.

[21] D. Orellana-Martín, L. Valencia-Cabrera, A. Riscos-Núñez, and M. J. Pérez-Jiménez, "A path to computational efficiency through membrane computing," *Theor. Comput. Sci.*, vol. 777, pp. 443–453, Jun. 2019.

[22] C. Yu, Q. Lian, D. Zhang, and C. Wu, "PAME: Evolutionary membrane computing for virtual network embedding," *J. Parallel Distrib. Computing*, vol. 111, pp. 136–151, 2018.

[23] Min Xie, Y. Du, P. Cheng, W. Wei, and M. Liu, "A cross-entropy-based hybrid membrane computing method for power system unit commitment problems," *Energies*, vol. 12, no. 3, p. 486, 2019. doi: 10.3390/en12030486.

[24] G. Zhang, J. Cheng, M. Gheorghe, and Q. Meng, "A hybrid approach based on differential evolution and tissue membrane systems for solving constrained manufacturing parameter optimization problems," *Appl. Soft Comput.*, vol. 13, no. 3, pp. 1528–1542, Mar. 2013.

[25] J. Xue and X. Liu, "Lattice based communication P systems with applications in cluster analysis," *Soft Comput.*, vol. 18, no. 7, pp. 1425–1440, Jul. 2014.
[26] J. Xue, X. Liu, and P. Chen, "Rhombic grid based clustering algorithm with spiking neural P systems," *J. Comput. Theor. Nanosci.*, vol. 13, no. 6, pp. 3895–3901, 2016.
[27] X. Liu and J. Xue, "A cluster splitting technique by Hopfield networks and P systems on simplices," *Neural Process. Lett.*, vol. 46, no. 1, pp. 171–194, Aug. 2017.
[28] H. Peng, P. Shi, J. Wang, A. Riscos-Núñez, and M. J. Pérez-Jiménez, "Multiobjective fuzzy clustering approach based on tissue-like membrane systems," *Knowl.-Based Syst.*, vol. 125, pp. 74–82, Jun. 2017.
[29] L. Huang, I. H. Suh, and A. Abraham, "Dynamic multi-objective optimization based on membrane computing for control of time-varying unstable plants," *Inf. Sci.*, vol. 181, no. 11, pp. 2370–2391, 2011.
[30] K. G. Subramanian, S. Sriram, B. Song, and L. Pan, "An overview of 2D picture array generating models based on membrane computing," in *Reversibility Universality*. Springer, 2018, pp. 333–356.
[31] C. Martín-Vide, G. Păun, J. Pazos, and A. Rodríguez-Patón, "Tissue P systems," *Theor. Comput. Sci.*, vol. 296, no. 2, pp. 295–326, 2003.
[32] X. Zhang, Y. Liu, B. Luo, and L. Pan, "Computational power of tissue P systems for generating control languages," *Inf. Sci.*, vol. 278, pp. 285–297, Sep. 2014.

JIE XUE received the B.S. and Ph.D. degrees in management science and engineering from Shandong Normal University, in 2010 and 2015, respectively, where she is currently an Associate Professor with Business School. Her research interests include machine learning, biocomputing, and medical image processing. She was a recipient of the National Visiting Scholar Program with the University of North Carolina, from 2017 to 2018.

SHUO YAN received the B.S. degree in information management and information system from Shandong Normal University, in 2017, where she is currently pursuing the M.S. degree in management science and engineering.

YUAN WANG received the bachelor's degree in management from the University of Qiqihar, in 2017. She is currently pursuing the master's degree in management science and engineering with Shandong Normal University.

TINGTING LIU received the B.S. degree from the Shandong University of Traditional Chinese Medicine, Jinan, China, in 1999, the M.S. degree from the Shandong Academy of Medical Science, and the Ph.D. degree from Shandong University, in 2009, all in medicine. Since 2018, she is currently a Professor with the Shandong Institute of Ophthalmology, Shandong Academy of Medical Sciences and Shandong Eye Hospital. Her research interests include retina and applications of OCT and optic nerve.

FENG QI received the B.S. degree in computer science and technology and the Ph.D. degree in information management and e-commerce from Shandong Normal University, Jinan, in 2005 and in 2011, respectively, where he has been an Associated Professor and the Dean of the Department of Electronic Commerce, since 2016. His main research interests include computational intelligence, data mining, and neural computing.

HONGYAN ZHANG received the B.S. degree in computer science technology from the Shandong University of Technology, Zibo, China, in 2004, the M.S. degree in computer application technology from Yantai University, Yantai, China, in 2007, and the Ph.D. degree in management science and engineering from Shandong Normal University, in Jinan, in 2011, where she has been a Lecturer with the Management Science and Engineering School, since 2012. Her research interests include the biological computing, intelligent computing, and data mining.

CHENGGONG QIU received the B.S. degree in computer science technology and the M.S. degree in computer application technology from Shandong Normal University, in 2003 and 2006, respectively, where he has been a Lecturer with the Management Science and Engineering School, since 2006. His research interests include machine learning and data mining.

JIANHUA QU received the B.S. degree in computer science and technology and the Ph.D. degree in information management and e-commerce from Shandong Normal University, in 2000 and 2010, respectively, where she has been an Associated Professor and the Dean of the Department of Information Management and Information System, since 2010. Her main research interests include computational intelligence and data mining.

XIYU LIU received the Ph.D. degree in mathematical science from Shandong University, Jinan, China, in 1990. He is currently the Dean of the Academy of Management Science and Engineering, Shandong Normal University, China. He is the author of two books and more than 140 articles. His research interests include membrane computing, data mining, computational intelligence, and nonlinear analysis. He was a recipient of the Taishan Scholar of Management Science and engineering, the Vice President of the Computer Education Research Association of China Higher Normal Universities, and the Vice President of the Shandong Computer Society.

DENGWANG LI received the B.S. and Ph.D. degrees in electronic engineering from Shandong University, in 2006 and 2011, respectively. He won the joint Ph.D. Program with the University of Sydney, from 2009 to 2010. He is currently a Professor with the Shandong Key Laboratory of Medical Physics and Image Processing, School of Physics and Electronics, Shandong Normal University. His research interests include signal processing and biomedical engineering.